THE JOURNAL OF PHYSICAL CHEMISTRY LETTERS
A JOURNAL OF THE AMERICAN CHEMICAL SOCIETY

pubs.acs.org/JPCL

Letter

Proton-Tunneling Dynamics along Low-Barrier Hydrogen Bonds: A Full-Dimensional Instanton Study of 6-Hydroxy-2-formylfulvene

Pablo E. Videla,* Lidor Foguel, Patrick H. Vaccaro,* and Victor S. Batista*

Cite This: *J. Phys. Chem. Lett.* 2023, 14, 6368−6375

Read Online

ACCESS | Metrics & More | Article Recommendations | Supporting Information

ABSTRACT: Understanding the dynamics of proton transfer along low-barrier hydrogen bonds remains an outstanding challenge of great fundamental and practical interest, reflecting the central role of quantum effects in reactions of chemical and biological importance. Here, we combine *ab initio* calculations with the semiclassical ring-polymer instanton method to investigate tunneling processes on the ground electronic state of 6-hydroxy-2-formylfulvene (HFF), a prototypical neutral molecule supporting low-barrier hydrogen-bonding. The results emerging from a full-dimensional *ab initio* instanton analysis reveal that the tunneling path does not pass through the instantaneous transition-state geometry. Instead, the tunneling process involves a multidimensional reaction coordinate with concerted reorganization of the heavy-atom skeletal framework to substantially reduce the donor−acceptor distance and drive the ensuing intramolecular proton-transfer event. The predicted tunneling-induced splittings for HFF isotopologues are in good agreement with experimental findings, leading to percentage deviations of only 20−40%. Our full-dimensional results allow us to characterize vibrational contributions along the tunneling path, highlighting the intrinsically multidimensional nature of the attendant hydron-migration dynamics.

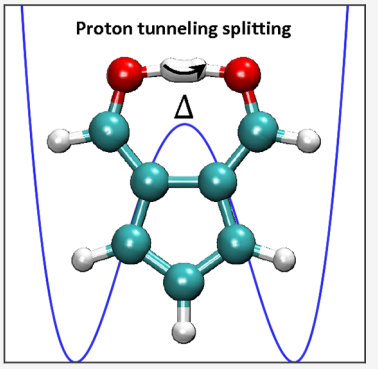

Proton transfer mediated by low-barrier hydrogen bonds (LBHBs), which support an extremely low potential-energy impediment for hydron migration, is a ubiquitous quantum-mechanical phenomenon that plays a central role in many reactions of chemical and biological importance.[1−4] In particular, fluctuating low-barrier hydrogen bonds have been proposed as essential elements of the molecular mechanisms of cooperativity and allosteric regulation in proteins.[5] Evidence for LBHBs in proteins can be traced back to reports of chemical shifts in ^{1}H NMR spectra that were significantly downfield shifted (17 and 21 ppm), with inverse fractionation factors (of about 0.3) suggesting a bond-order reduction of the transferring hydrogen that increased discrimination against deuterium in favor of an accumulation of protium when compared to analogous H-bonds in D_2O and H_2O.[6] Although LBHBs have been implicated in numerous biochemical pathways and have been explored extensively in condensed-phase environments, some controversy still exists regarding their putative roles in enzymatic catalysis.[7−16] The light mass of hydrogen makes it especially susceptible to nuclear quantum effects (NQEs), as well as to related phenomena arising from zero-point energy (ZPE) offsets and potential-energy surface (PES) anharmonicities, all of which can strongly modulate the overall efficiency and detailed pathway of the attendant proton-transfer events. Moreover, given the multidimensional character of tunneling-mediated pathways, intimate coupling among internal degrees of freedom can control both the mechanism and the rate of the ensuing dynamics. Even subtle displacements of heavy-atom centers in the complex of interest (e.g., donor/acceptor sites) can profoundly impact the nature of hydron migration.[17−20] As such, an accurate and quantitative description of NQEs has remained particularly challenging, since it requires an all-atom, all-electron simulation of the underlying dynamics.

Given the manifest importance of proton-transfer processes in chemistry and biochemistry, significant attention has focused on species containing intramolecular LBHBs, and their ability to discern the most salient geometric and electronic features that govern hydron migration. Recently, 6-hydroxy-2-formylfulvene (HFF) has emerged as a prototypical model system for the study of low-barrier hydrogen bonding (LBHBing) and associated hydron-transfer dynamics in neutral molecules.[21−23] As shown in Figure 1, HFF is characterized by a seven-membered reaction site in which a strong O···H···O intramolecular interaction is stabilized by π-electron conjugation with a cyclopentadiene ring. An atypical quasilinear hydrogen bond spans the short distance connecting hydroxymethylene (proton-donating) and formyl (proton-accepting) moieties, with a small potential-energy impediment for proton migration of ∼800 cm^{-1} giving rise to a vibrational

Received: May 16, 2023
Accepted: June 30, 2023
Published: July 7, 2023

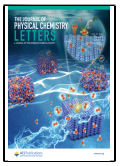

https://doi.org/10.1021/acs.jpclett.3c01337
J. Phys. Chem. Lett. 2023, 14, 6368−6375

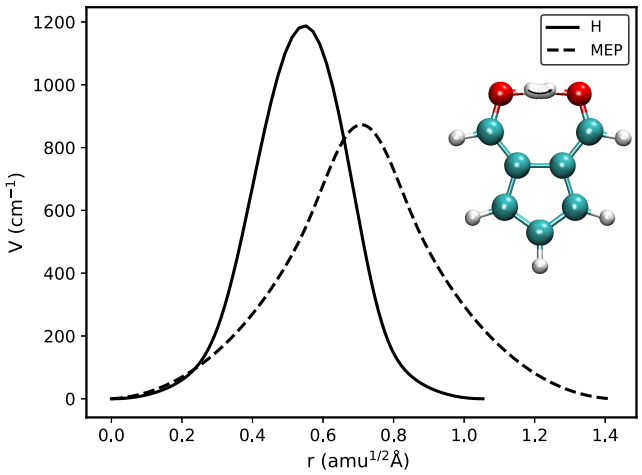

Figure 1. Potential-energy topography. Comparison of energy profile along the instanton path (H) and minimum-energy path (MEP). The inset shows a graphical representation of the instanton proton-tunneling path in HFF.

ZPE that putatively straddles the barrier crest.[22] Experimental measurements of tunneling-induced splitting for the vibrationless ($v = 0$) level of the $\tilde{X}^1A_1$ ground electronic state by Vealey et al.[21] provided a value of Δ_0^X(HFF) = 124.8 cm^{-1}, which represents the largest tunneling doublet ever reported for the ground electronic state of a neutral species. The characteristics of the LBHBing motif were confirmed by examining isotope effects, where deuteration of the labile proton caused a marked decrease in the tunneling splitting to Δ_0^X(HFF−d) = 36.4 cm^{-1}, leading to a deuterium kinetic isotope effect (DKIE) of $\Delta_0^X = \Delta_0^X(\text{HFF})/\Delta_0^X(\text{HFF−d})$ = 3.43 that bridges the metrics expected for above-barrier (classical-transport) and below-barrier (deep-tunneling) dynamics. From a theoretical perspective, investigations of proton-transfer dynamics conducted on potential-energy surfaces of reduced dimensionality (e.g., one-dimensional or two-dimensional) have provided invaluable insights, often enabling experimental trends to be reproduced in a qualitative or semiquantitative fashion.[24,25] The first reported *ab initio* study of the HFF ground electronic state by Millefiori and Alparone[24] employed the MP3/6-31G**//MP2/6-31G** methodology to find a proton-transfer barrier height of ∼1404 cm^{-1}, which, under the assumption of a one-dimensional reaction coordinate, led to a predicted tunneling splitting of 142 cm^{-1}. Subsequent calculations on unrelaxed two-dimensional reaction surfaces obtained at the MP2/6-31G** level of theory were performed by Tayyari et al.[25] These authors utilized the O−H stretching and O−H···O bending degrees of freedom as active modes, whereas all other coordinates remained fixed at their optimized equilibrium values. Such treatments revealed a substantial reaction impediment of ∼2274 cm^{-1} and an associated tunneling splitting of 167 cm^{-1}, with the latter displaying a strong dependence on the potential-energy cutoffs imposed upon the tunneling calculation. Nevertheless, the actual reaction mechanism is multidimensional in nature, and theoretical approaches based on reduced dimensions, which may be difficult to determine *a priori*, can lead to unforeseen complications that muddle the detailed interpretation of spectroscopic measurements.[26] As such, a comprehensive understanding of HFF tunneling dynamics in potential-energy surfaces of high dimensionality that serve to mediate the coupling among numerous modes of vibration still is lacking.

Here, we characterize proton-tunneling dynamics in the ground electronic state of HFF by using full-dimensional *ab initio* ring-polymer instanton (RPI) theory.[27−29] Ring-polymer instanton theory provides a computationally expedient semiclassical method suitable for unravelling the dynamics of barrier penetration in complex systems. In particular, the instanton represents the minimum-action path (with respect to the Euclidean imaginary-time action) that connects the reactants and the products, and has the ability to capture the effects of tunnelling and anharmonicity along the reaction pathway.[30,31] Aside from providing mechanistic insights into tunneling-mediated processes by identifying the optimal reaction path, RPI is a single-shot method that does not require detailed prior knowledge of the optimal tunneling path and can be performed on a complex system without the need to reduce dimensionality. The present implementation of this approach entails all-atom and all-electron quantum simulations that combine density-functional theory (DFT) treatments for the electronic degrees of freedom with an RPI approximation for the nuclear degrees of freedom to explore the unique hydron-migration processes of HFF in full dimensionality. Our full-dimensional analysis allows us to characterize the geometrical parameters, isotope effects, vibrational contributions, and multidimensional nature of proton migration through LHBHs.

We begin by analyzing the instanton path for proton tunneling in the ground electronic state of HFF as described in full dimensionality at the DFT level (see Methods). Given the exponential dependence of tunneling probability on the reaction barrier height, the choice of electronic structure method is very important for quantitative calculations of tunneling-induced splitting. Although highly accurate *ab initio* paradigms like CCSD(T) could be employed within the RPI formalism,[18] the extreme computational cost of such approaches often limits their direct practical implementation. Recent advances on machine-learning models that allow for the parametrization of potential-energy surfaces at a high level of theory can be employed to circumvent these challenges, although such analyses still are very demanding. Thus, a computationally expedient method that can reproduce the results of more accurate quantum-chemical calculations must be identified. In a recent study, Vealey et al.[22] performed an extensive comparison of reaction barriers for the ground electronic state of HFF predicted by using different electronic-structure methods and basis sets. The most accurate *ab initio* barrier height, as computed at the CCSD(T)/aug-cc-pvqz//CCSD(T)/aug-cc-pvdz level of theory, was found to be ΔE_{pt} = 870.5 cm^{-1}. Quite remarkably, DFT calculations performed with the ωB97X correlation-exchange functional[32] and aug-cc-pvdz basis set produced a reaction impediment of ΔE_{pt} = 873.1 cm^{-1}, in excellent agreement with the CCSD(T) result. Moreover, upon inclusion of harmonic zero-point energy contributions, the CCSD(T) and ωB97X methods both give ZPE-corrected barrier energies that essentially vanish, with values of −7.5 and −34.2 cm^{-1}, respectively. These results highlight the LBHBing nature of HFF, and suggest that the description of attendant normal modes is consistently captured at the CCSD(T) and ωB97X levels of theory.[22] In contrast, calculations performed with the B3LYP and M06-2X functionals underestimated the proton-transfer barrier by more than 400 cm^{-1} and predicted the vibrationless

https://doi.org/10.1021/acs.jpclett.3c01337
J. Phys. Chem. Lett. 2023, 14, 6368−6375

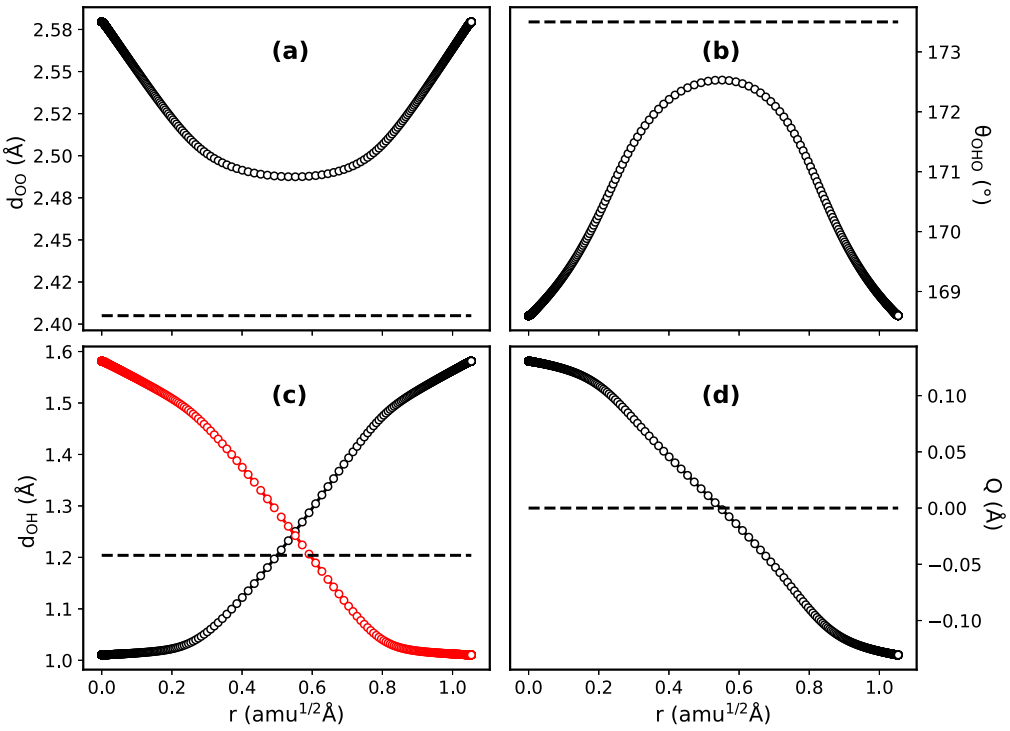

Figure 2. Changes in structure during proton tunneling. Geometrical parameters evaluated along the proton-tunneling path in the ground electronic state of HFF are depicted. Key structural metrics presented include (a) the oxygen donor−acceptor distance (d_{OO}), (b) the O−H···O hydrogen-bond angle (θ_{OHO}), (c) the two intramolecular O−H bond lengths (d_{O-H}, in black; $d_{O\cdots H}$, in red), and (d) the antisymmetrical π-electron delocalization metric,[34] $Q = (d_{C-O} - d_{C=O}) + (d_{C-C} - d_{C=C})$. Superimposed horizontal dashed lines correspond to the values of each parameter at the transition-state (TS) configuration.

level of HFF to be situated >250 cm^{-1} above the reaction impediment.[22] As such, the ωB97X functional is deemed to furnish a good compromise between accuracy and computational cost.

Figure 1 shows the energy profile along the instanton coordinate for the parent HFF molecule (see section 2 of the Supporting Information for energy profiles of isotopologues). A graphical representation of the instanton path is presented in the inset of the figure, where it can be observed that the labile H atom is most heavily involved in the proton transfer process. The instanton is based on a "least-action" principle (with respect to the Euclidean imaginary-time action),[27−29] and thus rigorously defines an optimal tunneling pathway that reveals the key steps of the proton-transfer mechanism. For comparison, Figure 1 also includes the shape of the potential-energy profile along the minimum-energy path (MEP), which corresponds to the trajectory of steepest descent from the apex of the barrier (i.e., the location of the transition state, TS). Of particular note is the fact that the instanton pathlength is shorter than that of the MEP at the expense of an increase in barrier height. This phenomenon occurs because the instanton does not pass through the saddle-point configuration of the TS, but rather chooses to cut the corner[33] and reduce the effective barrier width—a trade-off that results in a minimization of the action and an increase in the tunneling probability.

Changes in selected geometrical parameters of HFF along the instanton pathway are shown in Figure 2. The tunneling coordinate is found to be characterized by proton transfer restricted to the molecular plane (data not shown), with two different types of motion involved. The initial and final stages entail reorganization of the skeletal geometry to substantially shorten/lengthen the donor−acceptor distance (d_{OO}) and increase/decrease linearity of the O−H−O hydrogen-bond angle (θ_{OHO}), accompanied by less-pronounced motion of the transferring proton. In contrast, the intervening (or intermediate) step involves a fast transfer of the proton, as reflected by an increase (decrease) in the intramolecular O−H bond length ($d_{O\cdots H}$) with essentially negligible skeletal rearrangement. Figure 2 also depicts the π-electron delocalization metric proposed by Gilli and co-workers,[34] $Q = (d_{C-O} - d_{C=O}) + (d_{C-C} - d_{C=C})$, that affords a measure of resonance-assisted hydrogen bonding. In particular, this antisymmetrical coordinate shows the majority of electronic reorganization to occur during the intermediate proton-transfer stage. Such behavior mimics the hydron dynamics found in similar compounds such as malonaldehyde[27,35−37] and tropolone,[18,38−41] where distortion of the heavy-atom framework permits the system to attain an optimal geometry that reduces the effective tunneling pathlength. Remarkably, the instanton path does not pass through the transition-state configuration, as can be appreciated from the fact that the d_{OO} and θ_{OHO} structural parameters in Figure 2 never attain the TS values. This clearly highlights the "corner-cutting" effects intrinsic to the instanton.

Having located the requisite instanton pathway, the associated tunneling-induced splitting can be predicted by implementing the RPI approach.[27−29] Table 1 presents the ground-state tunneling metrics estimated for the parent HFF molecule as well as for two isotopologues involving replacement of the shuttling proton by a more massive deuteron or simultaneous substitution of the donor and acceptor oxygen centers by heavier ^{18}O atoms. Comparison with spectroscopic measurements performed on the H-atom and D-atom transfer reactions[21] shows the instanton

https://doi.org/10.1021/acs.jpclett.3c01337
J. Phys. Chem. Lett. 2023, 14, 6368−6375

Table 1. Ground-State Tunneling Splittings of HFF Isotopologues

Isotopologue	S ($\hbar$)	Δ^{calc} (cm^{-1})	Δ^{exp} (cm^{-1})
HFF (H)	3.99	172.8	124.8[a]
HFF (D)	4.97	44.1	36.4[a]
HFF (^{18}O)	4.03	170.4	---

[a]ref 21.

calculations to be in good agreement with experiments, reproducing observed trends and producing a near-quantitative deuterium kinetic isotope effect (DKIE) Δ_H/Δ_D of 3.9 relative to the experimental value of 3.4. In particular, deuterium substitution causes a significant reduction of the tunneling splitting, an effect mostly due to the $\sim\hbar$ increase in the instanton action. Further insights into the nature of isotope effects can be gleaned from atomic contributions to the total action, which can be calculated by recognizing that the squared mass-weighted pathlength is proportional to the corresponding action for tunneling.[27] Using this metric, the tunneling proton was found to yield roughly 60% of the total action, whereas the oxygen atoms accounted for an additional 20% (see section 2 of the SI). These results suggest that tunneling dynamics depend markedly on the isotopic form of the proton, with a small contribution arising from the rest of the molecular framework, an assertion confirmed by the analyses performed on the ^{18}O isotopologue (Table 1). Indeed, the introduction of ^{18}O produces a subtle reduction in the tunneling splitting, a result that can be rationalized by the modest contribution of oxygen atoms to the overall action as well as by the smaller mass ratio between oxygen and hydrogen isotopes (viz., 1.125 for ^{18}O/^{16}O versus 2 for D/H). Although measurements are not available for ^{18}O-substituted HFF, the high spectral resolution reported in previous studies[21,22] suggests that the RPI predictions should be amenable to experimental validation.

The theoretical tunneling metrics presented in Table 1 are in good agreement with experimental findings, although instanton predictions overestimate the magnitude of tunneling-induced splitting by ~20−40%. Two possible sources can contribute to this discrepancy. On the one hand, the computed tunneling splitting displays exponential sensitivity with the instanton action and inaccuracies in the potential-energy surface may introduce significant discrepancies. Recognizing that the action is proportional to the square-root of the potential energy, $S = \int \sqrt{2V}\, dr$,[27] an estimate of the error caused by the PES can be obtained by considering the ratio of the present DFT barrier height, ΔE_{pt} = 873.1cm^{-1}, to the best quantum-chemical barrier height currently available, ΔE_{pt} = 870.5 cm^{-1} as determined at the CCSD(T)/aug-cc-pvqz//CCSD(T)/aug-cc-pvdz level of theory.[22] Assuming a universal scaling of the PES, the excellent agreement that exists between the proton-transfer barriers obtained by DFT (using the ωB97X functional) and CCSD(T) indicates that the action should change by ~1.5% and the associated tunneling splitting would change by less than 2%. [Since the instanton does not pass through the transition-state geometry, it must be noted that any analysis based solely on the accuracy of the barrier height should be taken as a crude estimate.] Although more sophisticated correction methods that improve the accuracy of the PES along the actual instanton path can be considered,[42,43] this observation seems to preclude accuracy of the PES as the primary source of disagreement between experiment and theory.

The second source of error in the present analyses is rooted in the approximations inherent in the instanton approach. Indeed, although the instanton captures all of the anharmonicity along the instanton path, it neglects anharmonicities in the orthogonal direction by assuming harmonic fluctuations, an approximation that can fail for systems in which the ZPE is comparable to the potential barrier, making the ZPE-corrected barrier height vanishingly small (as certainly is the case in HFF). This assertion is reinforced by the fact that tunneling predictions for deuterated HFF are in closer agreement with experiments than those for the parent (undeuterated) species. To test the error introduced by the instanton approximation, we performed ancillary calculations of tunneling-induced splitting on analogous 1D and 2D potential-energy surfaces obtained for HFF, for which exact calculations can be performed (see section 3 of the SI). Even in this explicitly low-barrier regime, such analyses showed that the instanton approach was within 10−50% of the exact tunneling results. We remark that similar conclusions were obtained from reduced-dimensionality analysis of tunnelling splitting in the formic acid dimer.[26] It should be noted that removal of the harmonic approximation without resorting to reduced-dimensionality approaches would necessitate more demanding path-integral[44−48] or diffusion Monte Carlo[49,50] computations. Alternatively, the perturbatively corrected ring-polymer instanton theory recently introduced by Richardson and co-workers affords a novel approach for incorporating higher-order terms beyond those of the quadratic expansion.[51] It will be interesting to apply such methods to HFF in future studies.

To further characterize the multidimensional nature of the instanton and unravel vibrational contributions to the tunneling splitting of HFF, it proved instructive to perform a normal-mode decomposition along the instanton path.[36,52,53] Specifically, the instanton was projected along normal-mode displacement vectors determined at stationary points of the PES to decompose the contribution and coupling of each vibration to the tunneling dynamics. Two different sets of normal modes that offer complementary information were employed. First the normal modes of the minimum-energy configuration (MIN) were used to provide a description in terms of the vibrational motion at equilibrium. Figure 3 highlights the resulting projections of the instanton path along the subset of normal modes that undergo the largest displacement during the tunneling process (see section 1 of the SI for an analysis of normal modes). Detailed analysis of the displacement vectors associated with these specific degrees of freedom, shown schematically in the top panel of Figure 3, reveals two types of vibrations that couple most effectively to the reaction coordinate: (i) the OH stretching motion (ν_{34}^{MIN}) that promotes the proton transfer and (ii) modes associated with wagging of the OCCO framework (ν_4^{MIN}, ν_8^{MIN}, ν_{11}^{MIN}, ν_{12}^{MIN}) that substantially modulate the O···O donor−acceptor distance. It is worth pointing out that excitation of the ground-state vibration assigned to the ν_4^{MIN} wagging motion has been observed to produce a ~30% increase in tunneling-induced splitting (relative to that of v = 0),[21] thus highlighting the crucial role that this mode plays in governing the efficacy of proton migration.

Complementary information can be obtained by analyzing projections of the tunneling path along vibrations determined at the transition-state configuration, where the lone imaginary

https://doi.org/10.1021/acs.jpclett.3c01337
J. Phys. Chem. Lett. 2023, 14, 6368−6375

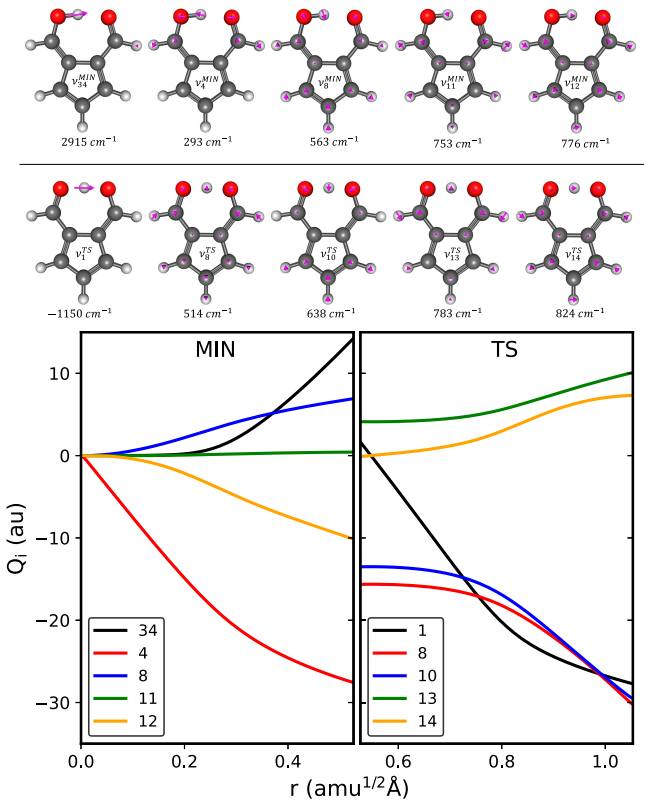

Figure 3. Effects of vibrational motion. The top panel presents displacement vectors for a subset of normal modes within the ground electronic state of HFF as computed for the minimum-energy (MIN) and transition-state (TS) configurations. The bottom panels display the projection of the instanton path along selected MIN (left) and TS (right) vibrational degrees of freedom.

mode (ν_1^{TS}) takes on the role of the tunneling reaction coordinate and thus provides a natural description of the proton-transfer event. We remark that the definitions of vibrational modes obtained at the transition-state configurations are different from their minimum-energy counterparts (see section 1 of SI). Figure 3 illustrates the projections along the instanton path for the subset of TS normal modes that have the largest contributions. In agreement with the previous discussion, motions that involved modulation of the O···O distance (ν_8^{TS}, ν_{10}^{TS}, ν_{13}^{TS},ν_{14}^{TS}) largely are activated during the tunneling process. In particular, detailed analyses of the normal-mode composition reveal that the selected TS degrees of freedom are correlated strongly with their MIN counterparts (see section 1 of SI). Specifically, the imaginary ν_1^{TS} mode correlates with the ν_{34}^{MIN} OH stretching mode, whereas modes ν_8^{TS}, ν_{10}^{TS}, ν_{13}^{TS} and ν_{14}^{TS} are correlated with ν_4^{MIN}, ν_8^{MIN}, ν_{11}^{MIN} and ν_{12}^{MIN}, respectively, although other degrees of freedom also contribute. Note that the results in Figure 3 also suggest two stages of skeletal rearrangement to take place before and after proton migration occurs, in line with the discussion from Figure 2. The fact that some displacements of the TS normal modes are not zero at the middle of the instanton path provides an additional manifestation of the aforementioned "corner-cutting" effects.

The results in Figure 3 reveal that various vibrational modes are activated during HFF tunneling dynamics and emphasize the multidimensional nature of the attendant proton-transfer process. This analysis also highlights the limitations of reduced-dimensionally schemes that demand the selection of one or more relevant reactive modes, the identification of which are difficult to make *a priori*.[24,25] Moreover, even modes that do not participate directly can affect the tunneling dynamics through ZPE contributions.[26] In this regard, the RPI methodology provides a general approach that can be employed in full dimensionality without requiring knowledge of the reaction path beforehand while still including the (harmonic) ZPE contributions of all modes.

In conclusion, we have theoretically investigated the dynamics of proton transfer through low-barrier hydrogen bonds, a motif common to many reactions of chemical and biological importance. In particular, *ab initio* calculations were combined with the ring-polymer instanton method to analyze isotopologues of 6-hydroxy-2-formylfulvene (HFF) in the $\tilde{X}^1A_1$ ground electronic state. We find that the tunneling-mediated path for hydron migration does not pass directly through the instantaneous transition-state geometry. Instead, the reaction involves concerted reorganization of the heavy-atom skeletal framework with a significant reduction of the donor−acceptor distance during the proton-transfer event. In fact, the intramolecular transformation is composed of three stages involving initial and final rearrangements of the heavy-atom skeletal framework to reduce the donor−acceptor distance combined with an intermediate stage, during which the ultrafast proton-transfer event occurs. This mechanism is supported by calculation of vibrationless ($v = 0$) tunneling-induced splitting for the H atom transfer reaction, which is found to be in good agreement with experimental data. Deuteration of the labile proton to form HFF-*d* leads to a significant reduction in tunneling probability, with a corresponding predicted DKIE of 3.9. Detailed analyses of vibrational modes that are active along the instanton path reveal that wagging motions of the OCCO reaction center, which modulate the crucial separation of donating and accepting oxygen moieties, are coupled strongly to the proton-tunneling process and thus play prominent roles in governing the efficacy of hydron migration.

METHODS

Tunneling splittings were computed using the ring-polymer instanton (RPI) method.[27−29] Within this formalism, the quantum-mechanical problem of determining the tunneling splitting in a molecule of N atoms is translated into a minimization problem on a classical phase-space of a linear polymer involving P replicas, or "beads", of the system. The beads are connected to nearest neighbors with harmonic springs and the effective potential of the linear polymer is given by:

$$U_P(\boldsymbol{R}) = \sum_{i=1}^{P} V(\boldsymbol{R}^{(i)}) + \sum_{i=2}^{P}\sum_{j=1}^{3N} \frac{m_j}{2(\beta_P\hbar)^2}(R_j^{(i)} - R_j^{(i-1)})^2$$

where $\beta_P = \beta/P$ and $\beta = 1/k_BT$. Here, $R_j^{(i)}$ denotes the j-th Cartesian coordinate of the i-th replica and $V(\boldsymbol{R}^{(i)})$ represents the potential energy associated with the i-th replica configuration. The instanton is defined as the path that minimizes $U_P(\boldsymbol{R})$ while connecting the double-well configurations. Once the instanton is located, the tunneling splitting is calculated as:

https://doi.org/10.1021/acs.jpclett.3c01337
J. Phys. Chem. Lett. 2023, 14, 6368−6375

$$\Delta = \left(\frac{2\hbar}{\phi}\right)\sqrt{\frac{S}{2\pi\hbar}}\, e^{-S/\hbar}$$

where $S = \beta_P \hbar U_P(\boldsymbol{R})$ represents the instanton action. The requisite determinant ratio, ϕ, controlling the prefactor follows from:

$$\phi = \frac{\prod_{i=1}^{3PN-7} \nu_i}{\prod_{i=1}^{3PN-6} \nu_i^0}$$

where ν_i represents the vibrational frequencies of the linear polymer connecting the double-well configurations (namely, the instanton) and ν_i^0 represents the frequencies of the configuration with the polymer collapsed to the bottom of one of the potential wells (namely, into the equilibrium position). We remark that the zero-frequency modes corresponding to overall translation, rotation, and, for the case of the instanton, cyclic permutation of the replicas is not included in the determinant ratio ϕ.

The full dimensional instanton path was located with an in-house code combining the L-BFGS algorithm[54] with on-the-fly, *ab initio* energy and force evaluations. Optimizations were performed in mass-weighted Cartesian coordinates, and convergence was achieved when the maximum absolute value of all components in the mass-scaled gradient was lower than 10^{-6} atomic units. Converged actions were obtained for $\beta\hbar$ = 16000 and P = 1024 (see section 2 of the SI for additional details). All electronic-structure calculations required to obtain energies and forces were performed at the density functional theory (DFT) level with the Gaussian 16 Rev. C01 software package[55] using the ωB97X functional[32] and the aug-cc-pvdz basis set.[56]

Decomposition of normal-mode contributions was performed according to the procedures elaborated elsewhere[36,52,53] by projecting the instanton path along the unit vectors in mass-scaled Cartesian coordinates associated with either the minimum-energy (MIN) or transition-state (TS) configuration (see section 2 of the SI). To reduce errors due to translations and rotations, the structures for the TS, MIN, and instanton were centered on their respective centers of mass and rotated to align the cyclopentadiene ring of HFF.

Reduced dimensionality calculations were performed on 1D and 2D potential energy surfaces. For the 1D calculation, the (relaxed) PES was constructed by scanning along the imaginary-frequency normal mode while relaxing all other degrees of freedom.[36] For the 2D calculations, in addition to the lone normal mode of the imaginary frequency, three modes related to the symmetric O···O breathing and C═O/HO−C wagging motions also were included separately. Exact tunneling splitting on these 1D/2D surfaces were obtained by performing imaginary time propagation using the SOFT method.[57,58]

■ ASSOCIATED CONTENT

Supporting Information

The Supporting Information is available free of charge at https://pubs.acs.org/doi/10.1021/acs.jpclett.3c01337.

Normal-mode analysis of HFF, additional computational details regarding the convergence of the instanton with respect to number of beads and temperature, and tunneling splitting calculations on 1D/2D potential energy surfaces (PDF)

■ AUTHOR INFORMATION

Corresponding Authors

Pablo E. Videla − *Department of Chemistry, Yale University, New Haven, Connecticut 06520, United States;* orcid.org/0000-0003-0742-0342; Email: pablo.videla@yale.edu

Patrick H. Vaccaro − *Department of Chemistry, Yale University, New Haven, Connecticut 06520, United States;* orcid.org/0000-0001-7178-7638; Email: patrick.vaccaro@yale.edu

Victor S. Batista − *Department of Chemistry, Yale University, New Haven, Connecticut 06520, United States;* orcid.org/0000-0002-3262-1237; Email: victor.batista@yale.edu

Author

Lidor Foguel − *Department of Chemistry, Yale University, New Haven, Connecticut 06520, United States*

Complete contact information is available at: https://pubs.acs.org/10.1021/acs.jpclett.3c01337

Notes

The authors declare no competing financial interest.

■ ACKNOWLEDGMENTS

L.F. and P.H.V. gratefully acknowledge support of the U.S. National Science Foundation (NSF) under the auspices of grants CHE-1464957 and CHE-2154840. V.S.B. acknowledges support from NSF Grant No. CHE-1900160 and high-performance computing time from the Yale High Performance Computing Center.

■ REFERENCES

(1) Giese, K.; Petković, M.; Naundorf, H.; Kühn, O. Multidimensional quantum dynamics and infrared spectroscopy of hydrogen bonds. *Phys. Rep.* **2006**, *430* (4), 211−276.

(2) *Hydrogen-Transfer Reactions*; Hynes, J. T., Klinman, J. P., Limbach, H.-H., Schowen, R. L., Eds.; Wiley-VCH Verlag GmbH & Co., 2007.

(3) Hibbert, F.; Emsley, J. Hydrogen bonding and chemical reactivity. In *Advances in Physical Organic Chemistry*; Bethell, D., Ed.; Vol. *26*; Academic Press, 1990; pp 255−379.

(4) Zundel, G. Hydrogen bonds with large proton polarizability and proton transfer processes in electrochemistry and biology. In *Advances in Chemical Physics*; Prigogine, I., Rice, S. A.John Wiley & Sons, Inc., 1999; pp 1−217.

(5) Dai, S.; Funk, L.-M.; von Pappenheim, F. R.; Sautner, V.; Paulikat, M.; Schröder, B.; Uranga, J.; Mata, R. A.; Tittmann, K. Low-barrier hydrogen bonds in enzyme cooperativity. *Nature* **2019**, *573* (7775), 609−613.

(6) Cleland, W. W.; Frey, P. A.; Gerlt, J. A. The low barrier hydrogen bond in enzymatic catalysis. *J. Biol. Chem.* **1998**, *273* (40), 25529−25532.

(7) Cleland, W. W.; Kreevoy, M. M. Low-barrier hydrogen bonds and enzymic catalysis. *Science* **1994**, *264* (5167), 1887−1890.

(8) Emsley, J. Very strong hydrogen bonding. *Chem. Soc. Rev.* **1980**, *9* (1), 91−124.

(9) Perrin, C. L.; Nielson, J. B. Strong" hydrogen bonds in chemistry and biology. *Annu. Rev. Phys. Chem.* **1997**, *48* (1), 511−544.

(10) Schiøtt, B.; Iversen, B. B.; Madsen, G. K. H.; Larsen, F. K.; Bruice, T. C. On the electronic nature of low-barrier hydrogen bonds in enzymatic reactions. *Proc. Natl. Acad. Sci. U.S.A.* **1998**, *95* (22), 12799−12802.

(11) Gerlt, J. A.; Kreevoy, M. M.; Cleland, W. W.; Frey, P. A. Understanding enzymic catalysis: The importance of short, strong hydrogen bonds. *Chem. Biol.* **1997**, *4* (4), 259−267.

(12) Graham, J. D.; Buytendyk, A. M.; Wang, D.; Bowen, K. H.; Collins, K. D. Strong, low-barrier hydrogen bonds may be available to enzymes. *Biochemistry* **2014**, *53* (2), 344−349.
(13) Warshel, A.; Papazyan, A.; Kollman, P. A. On low-barrier hydrogen bonds and enzyme catalysis. *Science* **1995**, *269* (5220), 102−106.
(14) Peter Guthrie, J. Short strong hydrogen bonds: Can they explain enzymic catalysis? *Chem. Biol.* **1996**, *3* (3), 163−170.
(15) Shokri, A.; Wang, Y.; O'Doherty, G. A.; Wang, X.-B.; Kass, S. R. Hydrogen-bond networks: Strengths of different types of hydrogen bonds and an alternative to the low barrier hydrogen-bond proposal. *J. Am. Chem. Soc.* **2013**, *135* (47), 17919−17924.
(16) Nadal-Ferret, M.; Gelabert, R.; Moreno, M.; Lluch, J. M. Are there really low-barrier hydrogen bonds in proteins? The case of photoactive yellow protein. *J. Am. Chem. Soc.* **2014**, *136* (9), 3542−3552.
(17) Castro, C.; Karney, W. L. Heavy-atom tunneling in organic reactions. *Angew. Chem.* **2020**, *59* (22), 8355−8366.
(18) Nandi, A.; Laude, G.; Khire, S. S.; Gurav, N. D.; Qu, C.; Conte, R.; Yu, Q.; Li, S.; Houston, P. L.; Gadre, S. R. Ring-polymer instanton tunneling splittings of tropolone and isotopomers using a δ-machine learned ccsd(t) potential: Theory and experiment shake hands. *J. Am. Chem. Soc.* **2023**, *145*, 9655.
(19) Redington, R. L.; Redington, T. E.; Blake, T. A.; Sams, R. L.; Johnson, T. J. O18 effects on the infrared spectrum and skeletal tunneling of tropolone. *J. Chem. Phys.* **2005**, *122* (22), 224311.
(20) Keske, J. C.; Lin, W.; Pringle, W. C.; Novick, S. E.; Blake, T. A.; Plusquellic, D. F. High-resolution studies of tropolone in the s and s 1 electronic states: Isotope driven dynamics in the zero-point energy levels. *J. Chem. Phys.* **2006**, *124* (7), 074309.
(21) Vealey, Z. N.; Foguel, L.; Vaccaro, P. H. Spectral signatures of proton-transfer dynamics at the cusp of low-barrier hydrogen bonding. *J. Phys. Chem. Lett.* **2018**, *9* (17), 4949−4954.
(22) Vealey, Z. N.; Foguel, L.; Vaccaro, P. H. Hydrogen-bonding motifs and proton-transfer dynamics in electronically excited 6-hydroxy-2-formylfulvene. *J. Phys. Chem. A* **2019**, *123* (30), 6506−6526.
(23) Foguel, L.; Vealey, Z. N.; Vaccaro, P. H. Spectroscopic signatures of low-barrier hydrogen bonding in neutral species. In *Spectroscopy and Computation of Hydrogen-Bonded Systems*; Wojcik, M. J., Ozaki, Y., Eds.; Wiley-VCH, 2023; pp 83−121.
(24) Millefiori, S.; Alparone, A. Ab initio study of the molecular structure, polarizability and first hyperpolarizability of 6-hydroxy-1-formylfulvene. *J. Chem. Soc., Faraday trans.* **1994**, *90* (19), 2873−2879.
(25) Tayyari, S. F.; Zahedi-Tabrizi, M.; Rahemi, H.; Mirshahi, H. A.; Emampour, J. S.; Rajabi, M.; Milani-Nejad, F. A two-dimensional potential function for bent hydrogen bonded systems. Ii-6-hydroxy-2-formylfulvene. *J. Mol. Struct.* **2005**, *730* (1), 17−21.
(26) Richardson, J. O. Full- and reduced-dimensionality instanton calculations of the tunnelling splitting in the formic acid dimer. *Phys. Chem. Chem. Phys.* **2017**, *19* (2), 966−970.
(27) Richardson, J. O.; Althorpe, S. C. Ring-polymer instanton method for calculating tunneling splittings. *J. Chem. Phys.* **2011**, *134* (5), 054109.
(28) Richardson, J. O. Perspective: Ring-polymer instanton theory. *J. Chem. Phys.* **2018**, *148* (20), 200901.
(29) Richardson, J. O. Ring-polymer instanton theory. *Int. Rev. Phys. Chem.* **2018**, *37* (2), 171−216.
(30) Benderskii, V. A.; Makarov, D. E.; Wight, C. A. *Chemical Dynamics at Low Temperatures*, Vol. *88*; John Wiley & Sons, Inc., 1994.
(31) Nakamura, H.; Mil'nikov, G. *Quantum Mechanical Tunneling in Chemical Physics*; CRC Press, 2013.
(32) Chai, J.-D.; Head-Gordon, M. Systematic optimization of long-range corrected hybrid density functionals. *J. Chem. Phys.* **2008**, *128* (8), 084106.
(33) Chapman, S.; Garrett, B. C.; Miller, W. H. Semiclassical transition state theory for nonseparable systems: Application to the collinear h+h2 reaction. *J. Chem. Phys.* **1975**, *63* (6), 2710−2716.
(34) Gilli, G.; Bellucci, F.; Ferretti, V.; Bertolasi, V. Evidence for resonance-assisted hydrogen bonding from crystal-structure correlations on the enol form of the.Beta.-diketone fragment. *J. Am. Chem. Soc.* **1989**, *111* (3), 1023−1028.
(35) Wang, Y.; Braams, B. J.; Bowman, J. M.; Carter, S.; Tew, D. P. Full-dimensional quantum calculations of ground-state tunneling splitting of malonaldehyde using an accurate ab initio potential energy surface. *J. Chem. Phys.* **2008**, *128* (22), 224314.
(36) Wang, Y.; Bowman, J. M. Mode-specific tunneling using the qim path: Theory and an application to full-dimensional malonaldehyde. *J. Chem. Phys.* **2013**, *139* (15), 154303.
(37) Wu, F.; Ren, Y.; Bian, W. The hydrogen tunneling splitting in malonaldehyde: A full-dimensional time-independent quantum mechanical method. *J. Chem. Phys.* **2016**, *145* (7), 074309.
(38) Murdock, D.; Burns, L. A.; Vaccaro, P. H. Vibrational specificity of proton-transfer dynamics in ground-state tropolone. *Phys. Chem. Chem. Phys.* **2010**, *12* (29), 8285−8299.
(39) Houston, P.; Conte, R.; Qu, C.; Bowman, J. M. Permutationally invariant polynomial potential energy surfaces for tropolone and h and d atom tunneling dynamics. *J. Chem. Phys.* **2020**, *153* (2), 024107.
(40) Vener, M. V.; Scheiner, S.; Sokolov, N. D. Theoretical study of hydrogen bonding and proton transfer in the ground and lowest excited singlet states of tropolone. *J. Chem. Phys.* **1994**, *101* (11), 9755−9765.
(41) Takada, S.; Nakamura, H. Effects of vibrational excitation on multidimensional tunneling: General study and proton tunneling in tropolone. *J. Chem. Phys.* **1995**, *102* (10), 3977−3992.
(42) Meisner, J.; Kästner, J. Dual-level approach to instanton theory. *J. Chem. Theory Comput.* **2018**, *14* (4), 1865−1872.
(43) Sahu, N.; Richardson, J. O.; Berger, R. Instanton calculations of tunneling splittings in chiral molecules. *J. Comput. Chem.* **2021**, *42* (4), 210−221.
(44) Marchi, M.; Chandler, D. Path-integral calculation of the tunnel splitting in aqueous ferrous−ferric electron transfer. *J. Chem. Phys.* **1991**, *95* (2), 889−894.
(45) Mátyus, E.; Althorpe, S. C. Calculating splittings between energy levels of different symmetry using path-integral methods. *J. Chem. Phys.* **2016**, *144* (11), 114109.
(46) Mátyus, E.; Wales, D. J.; Althorpe, S. C. Quantum tunneling splittings from path-integral molecular dynamics. *J. Chem. Phys.* **2016**, *144* (11), 114108.
(47) Vaillant, C. L.; Wales, D. J.; Althorpe, S. C. Tunneling splittings from path-integral molecular dynamics using a langevin thermostat. *J. Chem. Phys.* **2018**, *148* (23), 234102.
(48) Vaillant, C. L.; Wales, D. J.; Althorpe, S. C. Tunneling splittings in water clusters from path integral molecular dynamics. *J. Phys. Chem. Lett.* **2019**, *10* (22), 7300−7304.
(49) Suhm, M. A.; Watts, R. O. Quantum monte carlo studies of vibrational states in molecules and clusters. *Phys. Rep.* **1991**, *204* (4), 293−329.
(50) Gregory, J. K.; Clary, D. C. Calculations of the tunneling splittings in water dimer and trimer using diffusion monte carlo. *J. Chem. Phys.* **1995**, *102* (20), 7817−7829.
(51) Lawrence, J. E.; Dusek, J.; Richardson, J. O. Perturbatively corrected ring-polymer instanton theory for accurate tunneling splittings. *arXiv*, Apr. 21, 2023, arXiv:2304.10963, ver. 1. DOI: 10.48550/arXiv.2304.10963.
(52) Homayoon, Z.; Bowman, J. M.; Evangelista, F. A. Calculations of mode-specific tunneling of double-hydrogen transfer in porphycene agree with and illuminate experiment. *J. Phys. Chem. Lett.* **2014**, *5* (15), 2723−2727.
(53) Litman, Y.; Richardson, J. O.; Kumagai, T.; Rossi, M. Elucidating the nuclear quantum dynamics of intramolecular double hydrogen transfer in porphycene. *J. Am. Chem. Soc.* **2019**, *141* (6), 2526−2534.

https://doi.org/10.1021/acs.jpclett.3c01337
J. Phys. Chem. Lett. 2023, 14, 6368−6375

(54) Zhu, C.; Byrd, R. H.; Lu, P.; Nocedal, J. Algorithm 778: L-bfgs-b: Fortran subroutines for large-scale bound-constrained optimization. *ACM Trans. Math. Softw.* **1997**, *23* (4), 550−560.
(55) Frisch, M. J.; Trucks, G. W.; Schlegel, H. B.; Scuseria, G. E.; Robb, M. A.; Cheeseman, J. R.; Scalmani, G.; Barone, V.; Petersson, G. A.; Nakatsuji, H.; Li, X.; Caricato, M.; Marenich, A.; Bloino, j.; Janesko, B. G.; Gomperts, R.; Mennucci, B.; Hratchian, H. P.; Ortiz, J. V.; Izmaylov, A. F.; Sonnenberg, J. L.; Williams-Young, D.; Ding, F.; Lipparini, F.; Egidi, F.; Goings, J.; Peng, B.; Petrone, A.; Henderson, T.; Ranasinghe, D.; Zakrzewski, V. G.; Gao, J.; Rega, N.; Zheng, G.; Liang, W.; Hada, M.; Ehara, M.; Toyota, K.; Fukuda, R.; Hasegawa, J.; Ishida, M.; Nakajima, T.; Honda, Y.; Kitao, O.; Nakai, H.; Vreven, T.; Throssell, K.; Montgomery, J. A., Jr.; Peralta, J. E.; Ogliaro, F.; Bearpark, M.; Heyd, J. J.; Brothers, E.; Kudin, K. N.; Staroverov, V. N.; Keith, T.; Kobayashi, R.; Normand, J.; Raghavachari, K.; Rendell, A.; Burant, J. C.; Iyengar, S. S.; Tomasi, J.; Cossi, M.; Millam, J. M.; Klene, M.; Adamo, C.; Cammi, R.; Ochterski, J. W.; Martin, R. L.; Morokuma, K.; Farkas, O.; Foresman, J. B.; Fox, D. J. *Gaussian 16*, Revision c.01; Gaussian, Inc., Wallingford, CT, 2016.
(56) Kendall, R. A.; Dunning, T. H.; Harrison, R. J. Electron affinities of the first-row atoms revisited. Systematic basis sets and wave functions. *J. Chem. Phys.* **1992**, *96* (9), 6796−6806.
(57) Feit, M. D.; Fleck, J. A.; Steiger, A. Solution of the schrödinger equation by a spectral method. *J. Comput. Phys.* **1982**, *47* (3), 412−433.
(58) Kosloff, D.; Kosloff, R. A fourier method solution for the time dependent schrödinger equation as a tool in molecular dynamics. *J. Comput. Phys.* **1983**, *52* (1), 35−53.

https://doi.org/10.1021/acs.jpclett.3c01337
J. Phys. Chem. Lett. 2023, 14, 6368−6375